University of Huddersfield Repository

Evans, G., Shahzad, F., de Vries, E., Cavalletti, M., Iwnicki, S. and Bezin, Yann

An investigation of sleeper voids using a flexible track model integrated with railway multi-body dynamics

Original Citation

Evans, G., Shahzad, F., de Vries, E., Cavalletti, M., Iwnicki, S. and Bezin, Yann (2009) An investigation of sleeper voids using a flexible track model integrated with railway multi-body dynamics. Proceedings of the Institution of Mechanical Engineers, Part F: Journal of Rail and Rapid Transit, 223 (6). pp. 597-607. ISSN 0954-4097

This version is available at http://eprints.hud.ac.uk/id/eprint/14623/

The University Repository is a digital collection of the research output of the University, available on Open Access. Copyright and Moral Rights for the items on this site are retained by the individual author and/or other copyright owners. Users may access full items free of charge; copies of full text items generally can be reproduced, displayed or performed and given to third parties in any format or medium for personal research or study, educational or not-for-profit purposes without prior permission or charge, provided:

- The authors, title and full bibliographic details is credited in any copy;
- A hyperlink and/or URL is included for the original metadata page; and
- The content is not changed in any way.

For more information, including our policy and submission procedure, please contact the Repository Team at: E.mailbox@hud.ac.uk.

http://eprints.hud.ac.uk/

Proceedings of the Institution of Mechanical Engineers, Part F: Journal of Rail and Rapid Transit
http://pif.sagepub.com/

An investigation of sleeper voids using a flexible track model integrated with railway multi-body dynamics

Y Bezin, S D Iwnicki, M Cavalletti, E de Vries, F Shahzad and G Evans

Proceedings of the Institution of Mechanical Engineers, Part F: Journal of Rail and Rapid Transit 2009 223: 597
DOI: 10.1243/09544097JRRT276

The online version of this article can be found at:
http://pif.sagepub.com/content/223/6/597

Published by:
SAGE
http://www.sagepublications.com

On behalf of:
Institution of Mechanical Engineers

Additional services and information for *Proceedings of the Institution of Mechanical Engineers, Part F: Journal of Rail and Rapid Transit* can be found at:

Email Alerts: http://pif.sagepub.com/cgi/alerts

Subscriptions: http://pif.sagepub.com/subscriptions

Reprints: http://www.sagepub.com/journalsReprints.nav

Permissions: http://www.sagepub.com/journalsPermissions.nav

Citations: http://pif.sagepub.com/content/223/6/597.refs.html

>> Version of Record - Nov 1, 2009

What is This?

Downloaded from pif.sagepub.com at University of Huddersfield on August 24, 2012

An investigation of sleeper voids using a flexible track model integrated with railway multi-body dynamics

Y Bezin[1]*, **S D Iwnicki**[1], **M Cavalletti**[2], **E de Vries**[3], **F Shahzad**[3], and **G Evans**[4]
[1]Engineering & Technology Department, Manchester Metropolitan University, Manchester, UK
[2]VI-Grade, Perugia, Italy
[3]MSC.Software Limited, London, UK
[4]Corus Rail Technologies, Swinden Technology Centre, Moorgate, Rotherham, UK

The manuscript was received on 25 February 2009 and was accepted after revision for publication on 28 May 2009.

DOI: 10.1243/09544097JRRT276

Abstract: This article describes a flexible track system model (FTSM) that represents the track structure for a typical ballasted track, taking into account the flexibility of the rails, the sleeper mass and the resilience of the pad/fastening elements, as well as the ballast support stiffness condition. The detailed track model is integrated into a commercial railway vehicle dynamics software, thus allowing for any vehicle to be simulated onto the flexible track while at the same time taking into account the detailed calculation of the non-linear wheel–rail contact interaction. As an example, the application of the FTSM to the study of hanging sleepers, with respect to the UK Railway Group Standard limits, is presented. This example shows the impact of forces because of hanging sleepers on the vehicle and on the track, and attempts at quantifying the damage made to the track components for the specific conditions simulated.

Keywords: vehicle–track interaction, flexible track model, wheel–rail contact, hanging sleepers, void, track damage

1 INTRODUCTION

Multi-body system (MBS) software tools [**1**, **2**] are commonly used to simulate the dynamic behaviour of railway vehicles under various track and service conditions. In order to reduce the number of degrees of freedom of the system and to decrease simulation times, a simplified 'moving' track model is usually used in most commercial codes. These simplified track models are composed of a few spring-damper elements and suspended masses, independently modelled and coupled to every axle of the vehicle. This model representation has been extensively used to simulate long distances of track, and to predict vehicle behaviour and wheel–rail contact forces in the low-frequency domain [**3**].

However, with the increase of hardware capabilities and the development of standardized interfaces between MBS and finite element (FE) software, it has become possible to increase the level of detail of the track models used in railway MBS software by including more details of the track components as well as their flexibility. This offers the possibility to include higher-frequency effects into the vehicle–track interaction (VTI) models, which were shown by previous researchers [**4**–**7**] to be significant contributors to the development of certain types of degradation of the track components, e.g. corrugation.

This article first makes reference to existing reviews on VTI modelling, describing the various models used based either on MBS or FE techniques. The main disadvantages of using these two techniques separately are explained. This article then concentrates on the state-of-the-art in commercial MBS software that mostly use by default the 'moving track model', and refers to recent work looking at expanding the track modelling capabilities of this software.

A detailed flexible track system model (FTSM), newly developed in the software VI-Rail (MSC Adams) is then presented. It is used here to model a conventional ballasted track to predict the increase of wheel–rail contact forces due to hanging sleepers, whose gap size and numbers are defined on the basis of the UK Railway Group Standard limits.

*Corresponding author: Department of Engineering and Technology, Manchester Metropolitan University, Manchester, UK.
email: y.bezin@mmu.ac.uk

Downloaded from pif.sagepub.com at University of Huddersfield on August 24, 2012

2 MODELLING PRACTICE FOR VTI

2.1 Overview of VTI models in the wider context

Extensive reviews of VTI models and their applications are available from references [**6**], [**8**] and [**9**]. They range from beam on elastic foundation and beam on discrete flexible support with a single moving load to full three-dimensional FE models of the track and its substructure. Vehicle load is included as a moving force or a set of moving forces that represent different axles. They sometimes include harmonic dynamic loading through a spring-mass system representing the primary and/or secondary suspension of the vehicle. The wheel–rail normal contact problem is often approximated as a Hertzian spring. Most FE-based track models have in the past been limited to vertical dynamics because they have a partial representation of the vehicle system and they do not include a detailed wheel–rail contact routine that includes the definition of the creep forces in the contact plane. This is why more recent FE-based models have been used in combination with MBS software to produce more detailed information about the wheel–rail contact condition in the case; for example of a vehicle negotiating a switch and crossing, thus also considering the lateral dynamics, i.e. longitudinal and lateral creep forces [**10**].

2.2 Review of track models within railway vehicle MBS codes

2.2.1 Conventional 'moving' track models

A representation of a typical 'moving' track model is given in Fig. 1. Depending on the software used, each track subsystem travels along the track at the same speed as the vehicle and in the same plane as the wheelset it supports. There are usually three individual masses representing the left and right rails as well as the sleeper–ballast combined mass. They can have up to three degrees of freedom to account for the vertical and lateral displacement as well as the roll rotation about the direction of travel. Each degree of freedom is restricted by linear spring dampers. As mentioned before, this system offers the advantage of simplicity and therefore it speeds up the simulation process; however it does not represent:

(a) the rail bending and twisting behaviour;
(b) the individual pad and fastening properties;
(c) the individual sleepers mass and inertia;
(d) the interdependent deformation of adjacent track sections.

2.2.2 Latest development and introduction of 'discrete' flexible track models

Flexible track models taking into account the discrete nature of the track, i.e. taking into account every individual sleeper and rail fixing system as opposed to considering them as an homogenous continuum, have also been developed within MBS commercial software in the past few years [**11**]. This means that the range of application of typical vehicle MBS tools has been extended to the study of rather more local track geometry aspects and discontinuities, integrating the complete vehicle–track system into one modelling environment. This is the approach that was also taken for the model developed and presented in this article. A typical way of including the flexibility of the track elements is to generate the flexible component in an FE software and translate that element so

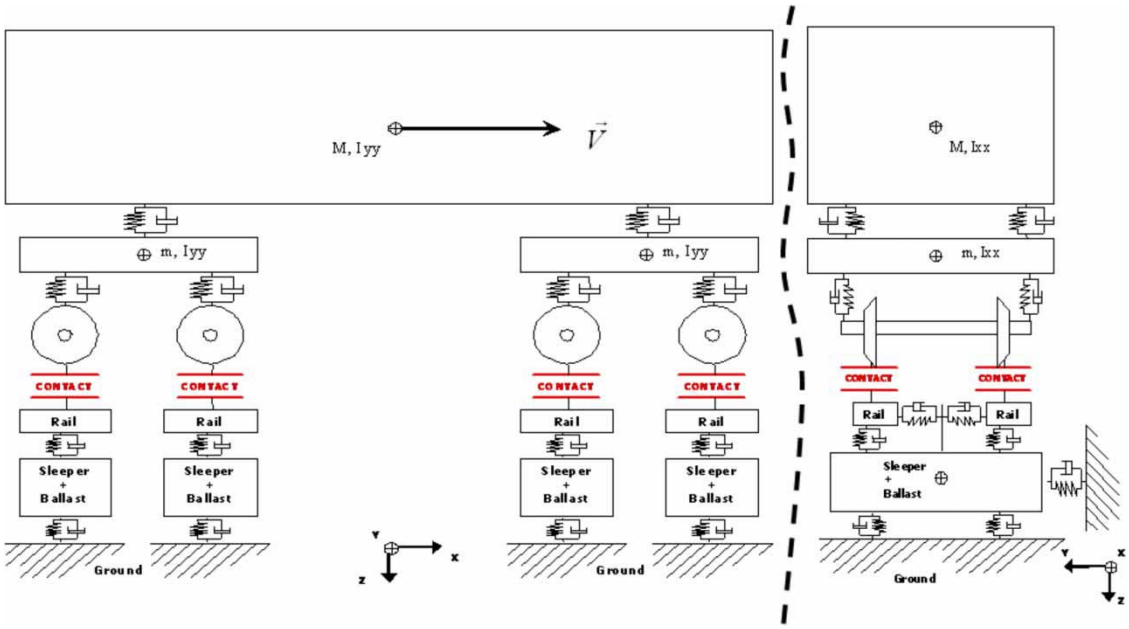

Fig. 1 Conventional 'moving track model' in MBS

Downloaded from pif.sagepub.com at University of Huddersfield on August 24, 2012

that it can be included within the MBS software for calculation. Early attempts made in Simpack and MSC Adams [**12**, **13**] included entire flexible structures built in FE and reduced to a set of modal coordinates and shape functions using a component mode synthesis method such as Craig–Bampton [**14**]. These earlier attempts were however limited to vertical dynamics and made use of simplified contact elements, i.e. linear spring–damper system. More recent development and case studies [**15**–**17**] have combined these flexible track models within MBS software, together with the more advanced contact algorithm that calculates the contact condition at every iteration time step, thus offering an integrated simulation of the complete vehicle track system for vertical as well as lateral dynamics, i.e. curving situations. This is the case of the FTSM presented here.

3 FLEXIBLE TRACK SYSTEM MODEL

3.1 Description of the FTSM

Starting from the 'moving' track model a more elaborate 'discrete' FTSM, illustrated in Fig. 2, was developed. The model takes into account:

(a) the left and right rail flexibility;
(b) every individual sleeper;
(c) every individual pad-fastening;
(d) individual ballast support to the sleepers.

3.1.1 Rail beams

Rails are modelled as beam elements that may be created in two ways.

1. Either using a simplified discrete series of concentrated mass above every sleeper, linked together by stiffness matrices representing Timoshenko equations. This element is one readily available from the MBS software library.
2. Or as an external beam generated from FE software and reduced to a set of normal modes and interface modes after linear mode analyses using the Craig–Bampton decomposition method. The rails include vertical and lateral bending modes as well as torsion modes. The boundary interface nodes are generated at the sleeper spacing distance to serve as attachment of the rails to the rest of the track.

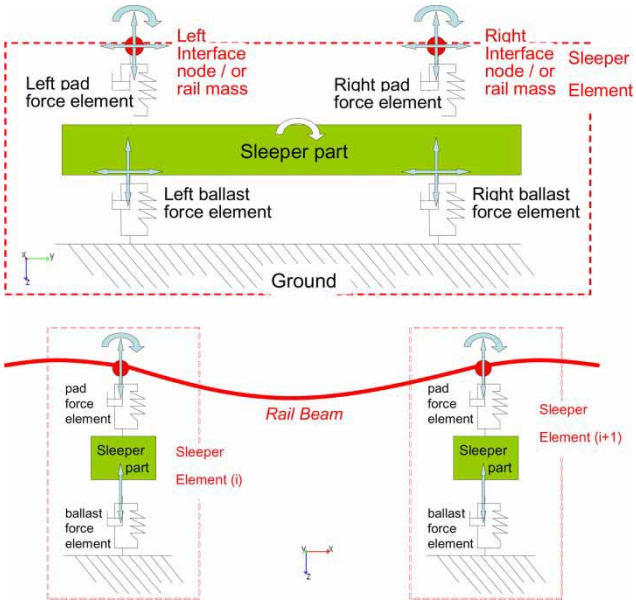

Fig. 2 Front (top) and side (bottom) views of FTSM

In both cases, interface markers are generated for the rails at positions above every sleeper and they are used to monitor the track response. Both models offer satisfying responses for low- to mid-range frequencies as shown in Fig. 3, showing the receptance graphs measured above sleepers, compared with a Timoshenko beam with discrete support using the modal summation approach [**18**]. The first two peak responses are identical at around 100 and 410 Hz for the rail bouncing on ballast, respectively, in phase and out of phase with the sleeper. All results presented in this article were generated using the first option above, which has the advantage of being simpler to model and faster to run because it is fully integrated within the MBS software. However because the rail is discretized into lengths equivalent to the sleeper spacing, it is only valid for frequencies up to a few hundred Hz and for predicting the track response above sleepers. The rail behaviour in between sleepers is approximated by the contact routine as explained in section 4 and it is not given as an output. The second option used in other studies that are not presented here is more accurate because it is generated from a discretized rail with 8–12 elements per sleeper spacing. It can therefore accurately represent the rail behaviour up the pinned–pinned frequency, typically from 1100 to 1200 Hz.

3.1.2 Sleepers

Sleepers are considered as rigid masses with three degrees of freedom for the vertical displacement, lateral displacement, and roll rotation.

3.1.3 Pads and fastenings

Force elements are created to attach the rails at each interface node situated above every sleeper. Linear stiffness and damping properties are defined for every individual element to restrain the five degrees of freedom of the rail beam interface nodes: lateral, vertical, roll, pitch, and yaw.

3.1.4 Sleeper to ballast interface

Two force elements are created per sleeper. They are situated underneath each rail. They are based on a linear spring–damper formulation that can also be

Downloaded from pif.sagepub.com at University of Huddersfield on August 24, 2012

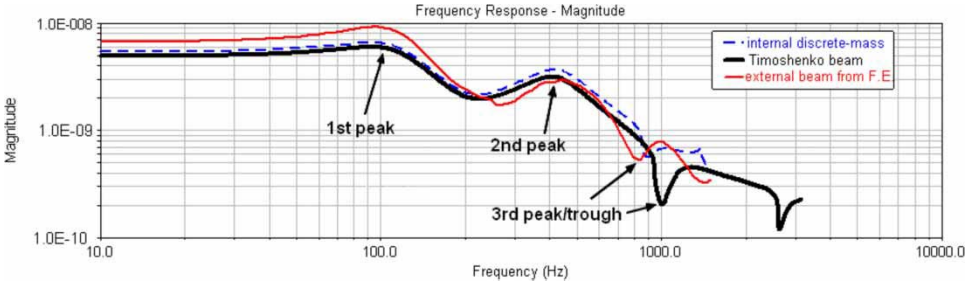

Fig. 3 Receptance graphs of track model using various rail beams (internal discrete-mass or external FE generated beams) compared with Timoshenko beam on discrete support

modified to include non-linearities according to displacement. This is used in the present case to model the sleeper void as explained later. Forces are generated for vertical and lateral degrees of freedom, and the pair of elements also restricts the roll rotation of the sleepers.

4 INTEGRATION WITH RAILWAY MBS DYNAMICS

The calculation process for the vehicle–track dynamic interaction was modified so that the wheel–rail contact algorithm can take into account the displacement of the rail due to the track flexibility for the calculation of the contact condition, and reciprocally apply the calculated forces onto the flexible track model. In essence, the rails are discretized into sections whose length corresponds to the sleeper spacing distance. Interface nodes are created at these locations and have to be used to calculate both the deformed shape of the rail and the force distribution onto the flexible track. Figure 4 shows the block diagram of the calculation process with the modified blocks consisting of:

(a) *force and torque distribution* onto adjacent rail nodes using a cubic shape function depending on the wheel position in between these two nodes;
(b) *flexible rail calculation* also using a cubic shape function based on adjacent rail nodes vertical position and pitch angle;
(c) *wheel–rail displacement and velocities* (based on the previous calculation and its derivative, and taking into account any input rail irregularity).

The wheel–rail contact condition is calculated from the wheel and rail profiles shape using a semi-Hertzian law [**19**]. The contact is discretized into a series of small thin strips to take into account the geometrical non-linearities within the contact patch, and a modified FASTSIM theory [**20**] is applied. This is the 'General' contact element available in the software VI-Rail.

5 FURTHER DISCUSSION ON THE MODEL

The flexible track is of a finite length and it is preceded and followed by rigid track sections. This allows the vehicle to enter the section of interest with the correct attitude in curving situations, i.e. correct wheelset yaw angle and lateral position with respect to track centre-line. The rail is usually pinned at both ends of the flexible section to minimize the unwanted peaks of forces at the transition. A minimum length of flexible track therefore needs to be modelled either side to allow for these forces to disappear and for which results can be discarded. The length can reasonably be estimated by using the characteristic length equation (1) and knowing that the distance at which the rail bending moment returns to zero is $1.25\,\pi.L$. This may range between 3 and 5 m depending on the rail pad and ballast stiffness. The total length of

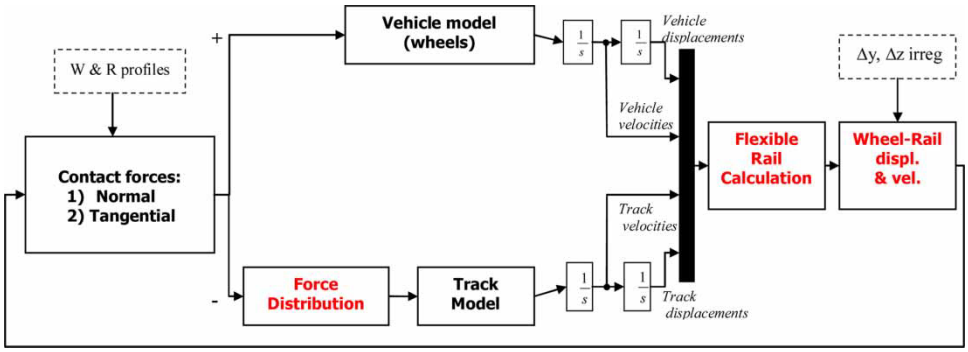

Fig. 4 Modified calculation process

Downloaded from pif.sagepub.com at University of Huddersfield on August 24, 2012

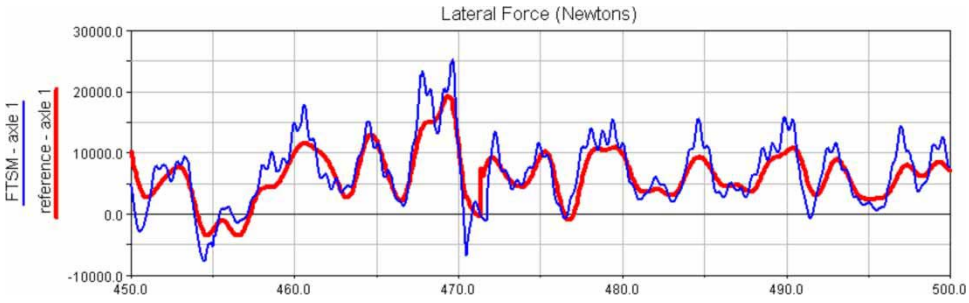

Fig. 5 Comparison between standard moving track model and FTSM

the flexible track generally modelled is therefore at least 10 times longer than this (50 m+), thus providing reasonable runtime.

Characteristic length

$$L = \sqrt[4]{\frac{4 \cdot E \cdot I}{k}} \tag{1}$$

where k is the foundation coefficient in N/m per meter of track, E the Young modulus in Pa, and I the second moment of area about the horizontal axis of the rail in m^4.

Figure 5 shows an example in the time domain of the lateral force obtained at the leading axle, with the discrete flexible track model compared with the standard moving track model, for the case of a UK class 91 locomotive model (214 kN axle load) running at 180 km/h in a 1428 m radius curve with 160 mm cant elevation. The run also includes measured vertical and lateral rail irregularities. The lower-frequency content matches well between the two runs; however the addition of the discrete sleepers and rail flexibility introduces a higher-frequency oscillation that corresponds to the sleeper passing wavelength. This results locally in higher peaks of forces up to 33 per cent in the present case. Note that a typical run of 50 m would take a few seconds with the standard moving track model, up to 10 min with the FTSM using simplified linear wheel–rail contact (sufficient for tangent track) and overnight with nonlinear contact described earlier (required for curving situation).

6 APPLICATION: DEFINITION OF A STUDY ON HANGING SLEEPERS

The FTSM was used to study the impact of voided sleepers on the wheel–rail contact forces and on the track forces. The case study and results are presented here, and Fig. 6 shows a snapshot of the model of a class 91 electric locomotive model used on a short section of flexible track. It includes 50 sleepers with a spacing of 65 cm and several voided sleepers.

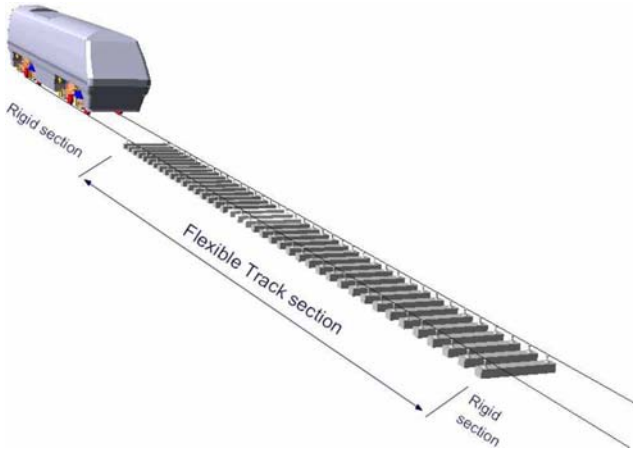

Fig. 6 Class 91 loco on voided flexible track

Table 1 Vehicle properties

	Class 91
Axle load	215 kN (×4 axles)
Unsprung mass per axle	2.9 mg
Sprung mass per bogie	4.5 mg
Bogie wheelbase	3.35 m
Bogie pivot spacing	10.5 m
Max. operating speed	200 km/h (125 mph)
Primary yaw stiffness (per axle)	22 MNm/rad
Primary vertical stiffness (per axle)	5.2 MN/m
Secondary vertical stiffness (per bogie)	2.3 MN/m

6.1 Vehicle model

A model of a class 91 electric locomotive was used on tangent as well as curved track. Typical characteristics for the vehicle are given in Table 1.

6.2 Definition of sleeper voids

According to the Network Rail Standard on Maintenance and Inspection of Permanent Way [**21**], the number of ineffective sleepers shall be as specified in Table 2, giving a maximum number of ineffective sleepers per 18 m of track ('number in length') with the maximum number of consecutive voided sleepers, i.e. otherwise separated by at least two sound sleepers ('number consecutive'). Different sequences of voided

Downloaded from pif.sagepub.com at University of Huddersfield on August 24, 2012

Table 2 Maximum number of ineffective sleepers

	Linespeed		
	Up to 60 mph	65–100 mph	105–125 mph
Number in length	6	3	1
Number consecutive			
Track radius >800 m	2	1	1
Track radius ⩽800 m	1	1	1

sleepers are therefore permissible based on the line speed. According to the minimum simulated speed: 96 km/h (60 mph), only up to three voided sleepers may be present, all separated by a minimum of two sound sleepers. Above 160 km/h (100 mph), only one voided sleeper may be present. Figure 7 illustrates the three and the one voided sleeper configurations with a close-up view of the gap.

In the simulation, the sleeper gap is modelled as a non-linear function based on displacement, which is illustrated in Fig. 8. As the sleeper is loaded and moves towards the ground, no force acts until a predefined gap is closed, and then a force that is proportional to displacement acts. The maintenance limit beyond which the track should not be allowed to deteriorate specifies a 7 mm gap between the sleeper and the ballast [**21**]. This value is used for all simulations and for all voided sleepers.

6.3 Simulation setup

Information used for the track model is given in Table 3. Note that no irregularity of the rail vertical and lateral alignment was considered, with the exception of the voids defined above. Table 4 provides the matrix of the simulation runs that were performed for

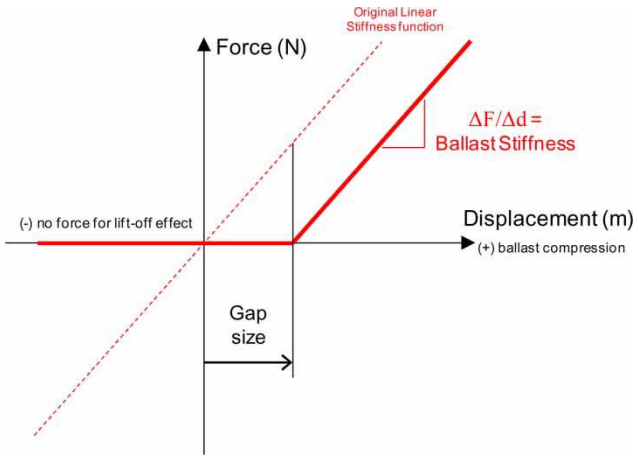

Fig. 8 Sleeper gap non-linear function

the case of the vehicle running on tangent track: set of speed and ballast support stiffness; and for the vehicle running on curved track: equivalent cant deficiency according to speed and curve radius.

7 ANALYSIS OF RESULTS

7.1 General interpretation

On all simulated cases, the voided sleeper is not able to support the vehicle axle load and it does not transfer any force to the ballast layer. Instead the force is distributed on the adjacent sleepers around the voided one. Figure 9 illustrates this pattern by displaying force vectors that are proportional to the force magnitude, in the case where the axle load is above sleeper i. The general pattern emerging is that of the nominal static axle force, named Fn, increasing slightly on sleepers $i+2$ and $i-2$ and increasing more significantly on

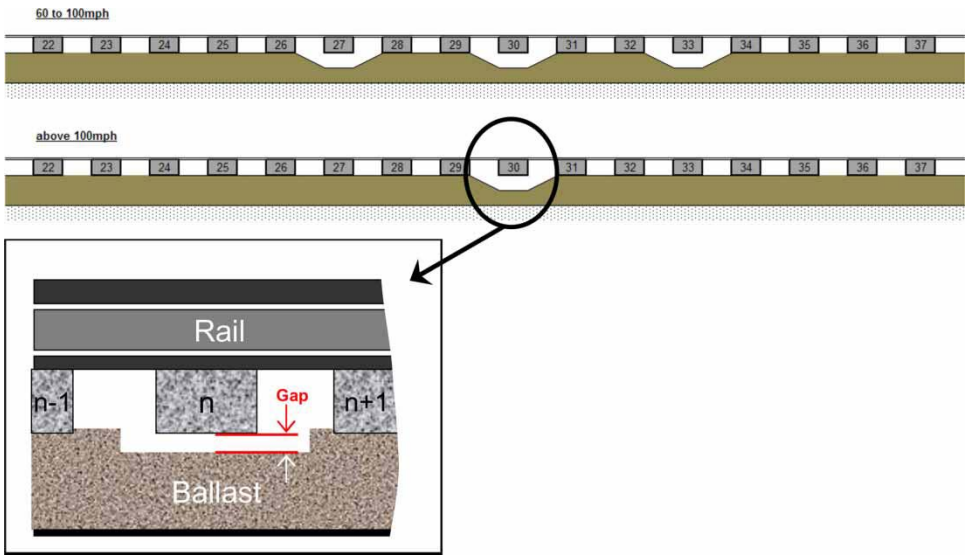

Fig. 7 One and three sleeper voids configuration with closeup view

Downloaded from pif.sagepub.com at University of Huddersfield on August 24, 2012

Table 3 Track and rail properties

Track	
Track gauge	1435 mm
Sleeper mass	308 kg
Sleeper roll inertia	127.7 kg m^2
Pad vertical stiffness/damping	200 kN/mm/98 kNs/m
Pad lateral stiffness/damping	280 kN/mm/58.6 kNs/m
Pad roll stiffness/damping	800 kN/rad/392 Ns/rad
Ballast stiffness on tangent track (depending on cases)	30, 60, and 100 kN/mm/sleeper end
Ballast stiffness on curved track	60 kN/mm/sleeper end (and 100 for the highest speed)
Ballast damping (60% critical)	9.06e4, 1.28e5, and 1.65e5 Ns/m per sleeper end
Rail	
Rail type	60 E1
Rail inclination	1 in 40
Rail material Young's modulus	210 kN/mm^2
Rail Poisson ratio	0.288
Rail section $I_{\text{horizontal}}$	3038 cm^4
Rail section I_{vertical}	512 cm^4
Rail section K_{torsion}	175 cm^4
Rail section area	7670 mm^2

sleepers $i+1$ and $i-1$. Sleepers further away do not seem to be affected by any force increase.

The other noticeable effect is speed dependent. As the speed increases, there is a more significant increase of the force on the sleeper that is situated just after the void, $i+1$, rather than on the one situated before, $i-1$. This can be explained by the inertia carried forward by the unsprung mass of the vehicle that tends to impact more heavily onto the rail after it has travelled over the voided sleeper.

7.2 Results on tangent track

Here the results obtained from the locomotive vehicle are analysed. The maximum increase in forces and stresses induced by the voids are given for:

(a) the wheel–rail contact normal force;
(b) the rail pad force;
(c) the sleeper to ballast interface force;
(d) the rail horizontal bending stress.

All percentage increases are quoted as the ratio of the maximum force or stress predicted on the voided track, divided by the nominal value for normal track condition. The maximum value is typically obtained at sleeper $i+1$ but all sleepers in the vicinity are also checked.

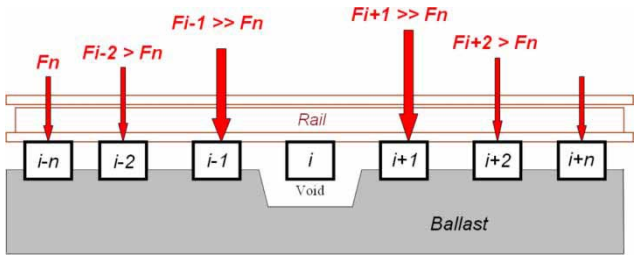

Fig. 9 Force distribution on voided track

7.2.1 *Wheel–rail contact forces*

The percentage increase of wheel–rail contact force is shown in Fig. 10 (triangles), together with the apparent trend (dashed line). The increase of normal force at the wheel–rail contact increases exponentially with speed with values varying between 10 per cent and 30 per cent. The ballast support stiffness has only a secondary effect with a small distribution about the trend line (there is a high correlation coefficient $r^2 = 0.927$). Note that the differentiation between the various stiffness cases is not highlighted in Fig. 10.

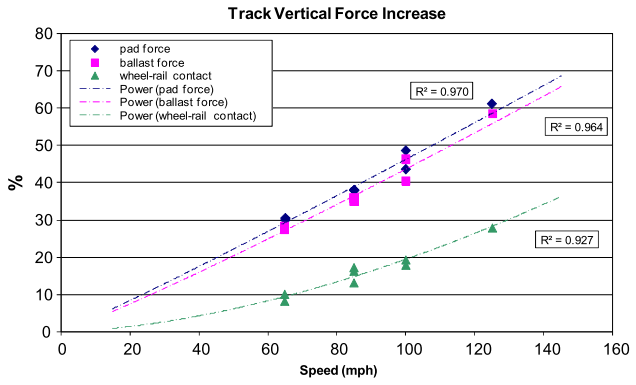

Fig. 10 Effect of sleeper void on wheel–rail contact and track forces on straight track

Table 4 Simulation run matrix

Simulation cases on tangent track							
Vehicle speed	km/h (mph)			105 (65)	137 (85)	161 (100)	201 (125)
Ballast support stiffness	kN/mm per sleeper end	30		✓	✓	–	–
		60		✓	✓	✓	–
		100		–	✓	✓	✓
Simulation cases on curved track							
Vehicle speed	km/h (mph)		88 (55)	105 (65)	137 (85)	161 (100)	201 (125)
			Corresponding cant deficiencies in mm				
Curve radius	m	550	18	85	252	–	–
		800	–	12	126	232	–
		1200	–	–	34	105	248

Downloaded from pif.sagepub.com at University of Huddersfield on August 24, 2012

7.2.2 *Track vertical forces*

Simulation values are shown in Fig. 10 as hollow squares and diamonds, respectively, for ballast and pad forces. The percentage increase of forces on the pad and on the ballast is far more significant than at the wheel–rail contact and it is linearly increasing with speed. The values range here between 30 per cent and 60 per cent increase. As for the case of wheel–rail contact forces, the ballast support stiffness is not the most significant factor (correlation coefficient of 0.964 and 0.97, respectively, for the ballast and the pad forces).

7.2.3 *Rail stresses*

Figure 11 shows the trend in rail stresses (All stresses in the article are quoted for the end fibre on the rail surface: rail foot for vertical bending and foot edge for lateral bending.) according to the ballast support stiffness, presenting both values for normal track condition and for voided track. As can be expected, soft support stiffness leads to higher bending stresses that reduce as the support stiffness increases, because less deflection of the rail around the void is allowed. Note that all values predicted here remain below 100 MPa, which is well below the yield limit for rail steel; however a low support condition may affect the life of the rail especially in case defects are present in the rail such as corrosion pit for example. Figure 12 shows the percentage increase for all simulated cases. The percentage appears to increase with ballast support stiffness and it also increases with speed. Values range between 22 per cent and 42 per cent.

7.3 Results on curved track

As observed for tangent track, the same reduction of force occurs above the voided sleepers leading to an increase on the adjacent sleepers. Because of the curving forces and the vehicle steering ability, the high rail (towards the outside of the curve) and the low rail (towards the inside of the curve) do not experience the same forces, and the various cant deficiencies and speed simulated give rise to different results.

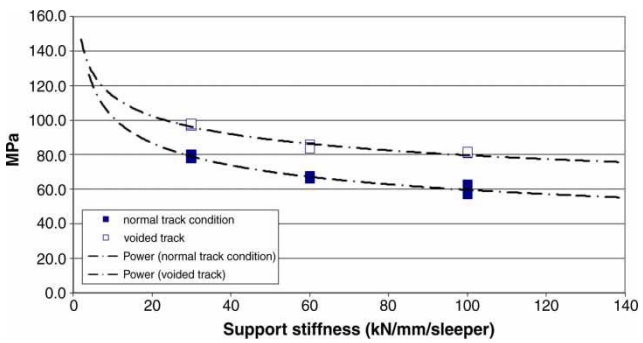

Fig. 11 Vertical bending stress prediction against ballast support stiffness on straight track

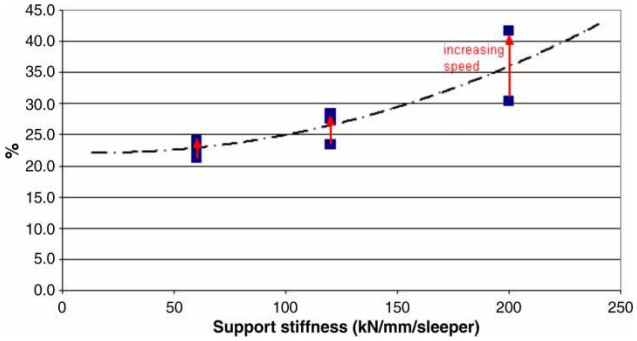

Fig. 12 Vertical bending stress percentage increase against support stiffness on straight track

7.3.1 *Wheel–rail contact forces*

The wheel–rail normal contact pressure and derailment quotient (lateral by vertical force ratio) were monitored. The normal pressure increases as the wheel travels over the void and reaches the next sound sleeper. This increase is exacerbated on the high rail due to the cant deficiency and the uncompensated centrifugal forces. The percentage difference increases with speed up to a maximum of 13 per cent. The derailment ratio reaches a maximum value of 0.34 out of all the simulated cases. This is well below the Nadal limit of 1.2. The presence of voids only increases the ratio by a quantity ranging between 3 per cent and 8 per cent.

7.3.2 *Vertical track forces*

With the increasing speed and increasing cant deficiency and due to the non-compensated centrifugal forces, the high rail experiences a force increase while the low rail experiences a decrease. Introducing voided sleepers in these conditions give rise to increased forces that are of the same magnitude on both high and low rails, i.e. between 26 per cent and 67 per cent, respectively, for 550 m radius curve at 55 mph and 1200 m radius curve at 125 mph. The ballast forces also increase with speed and cant deficiency between 25 per cent and 59 per cent, and the largest curve shows the most susceptibility, as shown in Fig. 13.

7.3.3 *Lateral track forces*

In the lateral direction, the same observations are made with increasing force and increasing percentage with speed and cant deficiency. The larger curve is also more sensitive to the increase of lateral forces. This is shown in Fig. 14.

7.3.4 *Rail stresses*

The maximum vertical bending stresses are imposed onto the high rail as the cant deficiency and speed increases, because of the weight shift onto the high rail. The magnitude of the predicted stresses is very

Downloaded from pif.sagepub.com at University of Huddersfield on August 24, 2012

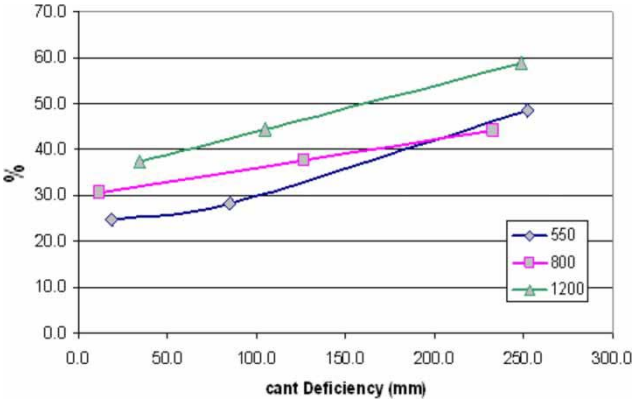

Fig. 13 Percentage increase in ballast vertical forces on curved track for 550 m (diamond), 800 m (square), and 1200 m (triangle) radius curves

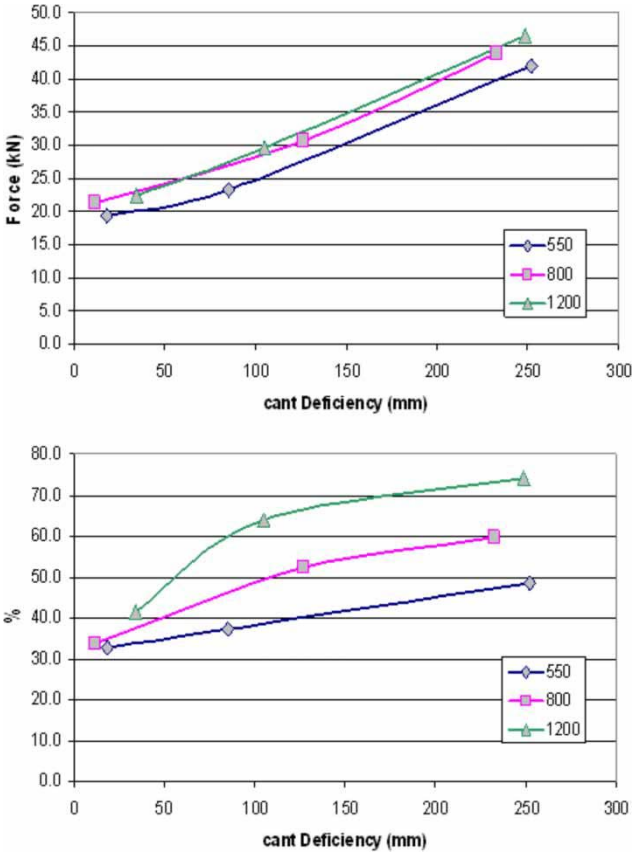

Fig. 14 Ballast lateral force (top) and percentage increase (bottom) on curved track for 550 m (diamond), 800 m (square), and 1200 m (triangle) radius curves

consistent, i.e. they do not vary with the curve radius but mainly with the cant deficiency. The percentage increase because of voided sleepers is also very consistent for all simulated cases with values ranging between 35 per cent and 40 per cent.

Lateral bending stresses within the rail are not as straight forward to interpret because they are governed by the complex behaviour of the vehicle model suspensions and the resulting wheel–rail contact condition. However some trends are noticeable from the magnitude of the maximum stresses plotted in Fig. 15.

1. Stresses increase with increasing cant deficiency.
2. At around 100 mm cant deficiency, stresses in both high and low rails are very similar and consistent for all simulated curves, i.e. just below 80 MPa.
3. Above 100 mm cant deficiency, the stresses on the high rail become higher than on the low rail and the smaller radius curves, i.e. 550 and 800 m, return the highest stresses.

The percentage increases because of the sleeper voids are plotted in Fig. 16. Trends are difficult to extract from this plot because the percentage increases are highly variable, i.e. between 11 per cent and 66 per cent. However it seems that towards the higher

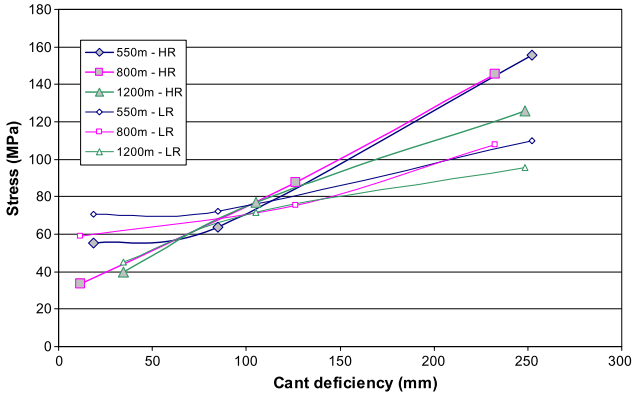

Fig. 15 Rail lateral bending stress on curved track for 550 m (diamond), 800 m (square), and 1200 m (triangle) radius curves, on high rail (HR) and low rail (LR)

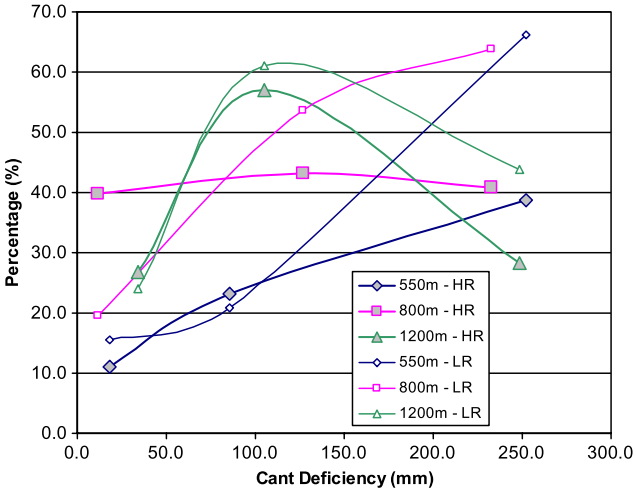

Fig. 16 Percentage increase in rail lateral bending stress on curved track for 550 m (diamond), 800 m (square), and 1200 m (triangle) radius curves, on high rail (HR) and low rail (LR)

Downloaded from pif.sagepub.com at University of Huddersfield on August 24, 2012

cant deficiencies the low rail sees a larger increase than the high rail for a specific curve radius (although the magnitude remains lower as shown in Fig. 15).

1. For the high rail on the 550 m radius curve, the percentage difference increases with cant deficiency (from 11 per cent to 39 per cent).
2. For the high rail on the 800 m radius curve, the percentage difference remains more or less constant (around +40 per cent).
3. For the high rail on the 1200 m radius curve, the percentage difference reaches a peak at 100 mm cant deficiency (57 per cent).

This shows that the percentage increase in lateral rail bending stress depends greatly on the curve radius considered.

8 CONCLUSION

An FTSM has been developed within one commercial railway multi-body dynamics software. It allows the detailed modelling of a ballasted track to be achieved by considering the flexibility of the rails, the individual rail pad supports, individual sleepers, and their local ballast support. The vehicle–track dynamic interaction can thus be simulated to predict the effect of track defects such as sleeper voids on the forces generated at the wheel–rail contact and within the track structure. This article presents the application of the vehicle–track model to the analysis of the wheel–rail contact and track forces in the presence of hanging sleepers modelled with reference to the UK Railway Group Standard limit for maintenance. A locomotive model running from mid to high speeds is used on tangent track and in various curving situations to investigate the effect of curve radii and cant deficiencies in the presence of voided sleepers. The main conclusions are as follows.

8.1 Contact forces

The selected simulation conditions showed that the increase of contact forces can be of the order of 10–30 per cent for mid to high speeds, in the presence of voided sleepers such as those described within the Railway Group Standard limit for maintenance. This is in agreement with the necessity of imposing speed restriction once these limits are exceeded, in order to maintain the damaging track forces within a reasonable level.

8.2 Track forces

The effect of sleeper voids was proved to have a far more significant effect on the forces imposed on the track components than on the wheel–rail contact. The increase of forces and stresses experienced by rail pads and by the ballast is similar. For the vehicle running from mid to high speeds, the dominant factor is the velocity and under the conditions simulated here, the increase is of the order of 30–60 per cent.

8.3 Rail stresses

Sleeper voids also tend to increase the stresses experienced by the rail in the vicinity of the void. The maximum increase is observed for the higher speeds (nearing 40 per cent). Although stiffer track support conditions give rise to higher stress increases, they are also responsible for a lower global deformation of the rail and therefore lower stress levels. Overall the predicted increase, although high, does not reach a level that may be considered close to the yield strength of the material. However the life of the rail may be significantly affected in the presence of a voided sleeper especially if internal defects are also present in the rail.

8.4 Curving situations

The presence of voided sleepers in curves means that in the vertical direction, there is an imbalance between the high and the low rail, and in the lateral direction, higher forces are generated. The voids increase the forces on the track and therefore the levels of bending stresses in the rail.

The increase of track forces in the lateral direction is significant and it further increases with the cant deficiency to a maximum of 60–75 per cent, depending on the curve radius. This higher level of forces on the ballast results in increased local stresses on the ballast underneath the sleepers around the voided one. This may lead to further sleepers becoming voided as well as to weak resistance of the track to lateral shift.

9 FURTHER DISCUSSION

From the results presented in this article and particularly the increased forces predicted on the track and plotted in Fig. 10, it can be noticed that a defect present in the track lead to an increase in forces that is far more important on the track components, i.e. rail pads and ballast, than on the wheel rail contact. This highlights the necessity of having detailed track models in order to carry out track damage analyses, and shows that using simplified track models to predict wheel–rail contact forces and using them as input to third-party track damage models may lead to under-estimate the damage made by these forces.

10 FUTURE DEVELOPMENT

The analyses presented in this article may benefit from further improvement to the modelling methods used

Downloaded from pif.sagepub.com at University of Huddersfield on August 24, 2012

to improve the simulation speed and increase the number of parameters investigated, e.g. axle loads, speeds, curve types, etc, leading to a more comprehensive analysis. Additionally, the results may be influenced by the addition of a flexible wheelset, which would require extensive development of the model at this stage and is planned as future research work. If rail stresses are to be considered in more detail, other stresses such as residual, temperature, and contact stresses would need to be included.

ACKNOWLEDGEMENT

The authors would like to thank the UK Engineering and Physical Sciences Research Council (EPSRC) and the Technology Strategy Board (TSB) for funding the development of the FTSM. The significant contribution and support from the project partners: MSC Software (VI-Grade), Corus, Network Rail, and Carillion Rail is also acknowledged.

© Authors 2009

REFERENCES

1 **Garg, V. K.** and **Dukkipati, R. V.** *Dynamics of railway vehicle systems*, 1984, p. 407 (Academic Press, Canada).
2 **Iwnicki, S.** *Handbook of railway vehicle dynamics* (Ed. S. Iwnicki), 2006, p. 776 (Taylor & Francis Group, Boca Raton, Florida, USA).
3 **Evans, J.** and **Iwnicki, S. D.** *Vehicle dynamics and the wheel/rail interface*. In Proceedings of the IMechE Seminar on *Wheels on rails – an update*, London, UK, 2002.
4 **Grassie, S. L.** Model of a railway track and train–track interaction at high frequencies: results of benchmark test. *Veh. Syst. Dyn.*, 1996, **25** (Supplement), 243–262.
5 **Knothe, K.** and **Grassie, S.** Modelling of railway track and vehicle–track interaction at high frequencies. *Veh. Syst. Dyn.*, 1993, **22**(3–4), 209–262.
6 **Nielsen, J. C. O., Lunden, R., Johansson, A.,** and **Vernersson, T.** Train–track interaction and mechanisms of irregular wear on wheel and rail surfaces. *Veh. Syst. Dyn.*, 2003, **40**(1–3), 3–54.
7 **Popp, K., Kruse, H.,** and **Kaiser, I.** Vehicle–track dynamics in the mid-frequency range. *Veh. Syst. Dyn.*, 1999, **31**, 423–464.
8 **Dahlberg, T.** *Railway track dynamics – a survey*, 2003 (Division of Solid Mechanics, IKP, Linköping University, Linköping, Sweden).
9 **Popp, K., Knothe, K.,** and **Pöpper, C.** System dynamics and long-term behaviour of railway vehicles, track and subgrade: report on the DFG Priority Programme in Germany and subsequent research. *Veh. Syst. Dyn.*, 2005, **43**(6–7), 485–521.
10 **Kassa, E., Andersson, C.,** and **Nielsen, J. C. O.** Simulation of dynamic interaction between train and railway turnout. *Veh. Syst. Dyn.*, 2006, **44**(3), 247–258.
11 **Elkins, J., Brickle, B., Wilson, N., Singh, S.,** and **Wu, H.** Track structure modeling with Nucars and its validation. *Veh. Syst. Dyn.*, 2002, **37** (Supplement), 420–431.
12 **Dietz, S., Hippman, G.,** and **Schupp, G.** Interaction of vehicle and flexible tracks by co-simulation of multibody vehicle systems and finite element track models. *Veh. Syst. Dyn.*, 2002, **37** (Supplement), 372–383.
13 **Zacher, M.** and **Ambrogi, F.** Dynamics of a train over a flexible bridge. In Proceedings of the 15th European Mechanical Dynamics User Conference, Roma, Italy, 2000.
14 **Craig, R. R.** and **Bampton, M. C. C.** Coupling of substructures for dynamics Analyses. *AIAA J.*, 1968, **6**(7), 1313–1319.
15 **Bezin, Y.** Development of a flexible track model and its application to advance railway track design. In Proceedings of the 1st VI-Grade User Conference, Marburg, Germany, 2007.
16 **Gonzalez, F. J., Suarez, B., Paulin, J.,** and **Fernandez, I.** Safety assessment of underground vehicles passing over highly resilient straight track in the presence of a broken rail. *Proc. IMechE, Part F: J. Rail and Rapid Transit*, 2008, **222**(F1), 69–84. DOI: 10.1243/09544097JRRT128.
17 **Shu, X., Wilson, N.,** and **Sasaoka, C.** Development of a real-time wheel/rail contact model in NUCARS and application to diamond crossing and turnout design simulations. In Proceedings of the 19th IAVSD Symposium 2005, Milan, Italy, 2005.
18 **Xie, G.** and **Iwnicki, S. D.** Simulation of wear on a rough rail using a time-domain wheel–track interaction model. *Wear*, 2008, **265**(11–12), 1572.
19 **Kik, W.** and **Piotrowski, J.** A fast, approximate method to calculate normal load at contact between wheel and rail and creep forces during rolling. In Proceedings of the 2nd Mini Conference on *Contact mechanics and wear of wheel/rail systems*, TU Budapest, 1996.
20 **Kohl, C.** *Modifikationen zum Kalkerschen Programm FASTSIM für die vereinfachte Theorie des rollenden Kontaktes*. Inst. für Luft- und Raumfahrt, Technische Universität Berlin, 1982.
21 *Inspection and maintenance of permanent way, NR/SP/TRK/001*. 2005, Network Rail.

Downloaded from pif.sagepub.com at University of Huddersfield on August 24, 2012